A Refined Understanding of the Ice Cloud Longwave Scattering Effects in Climate Model

Chongxing Fan[1]*, Yi-Hsuan Chen[1+], Xiuhong Chen[1], Wuyin Lin[2], Ping Yang[3], Xianglei Huang[1]

[1] Department of Climate and Space Sciences and Engineering, the University of Michigan, Ann Arbor, Michigan, USA

[2] Environmental & Climate Sciences Department, Brookhaven National Laboratory, New York State, USA

[3] Department of Atmospheric Sciences, Texas A&M University, Texas, USA

* Corresponding Author: Chongxing Fan (cxfan@umich.edu)

[+] Current affiliation: Research Center for Environmental Changes, Academia Sinica, Taipei, Taiwan

Key Points

- Ice-cloud longwave (LW) scattering leads to warming with a pattern similar to the response to quadrupled CO_2 in E3SM version 2.
- Strong Arctic warming is part of the global response to radiative perturbation rather than a local impact of LW scattering.
- Including ice-cloud LW scattering does not significantly affect the simulated responses to abrupt 4×CO_2 increases.

Submitted to *Journal of Advanced Modeling Earth Systems*

Original submission on November 5, 2022

Resubmission on May 7, 2023

Revision on August 23, 2023

Abstract

Because longwave (LW) absorption by greenhouse gases and clouds is more significant than the LW scattering effect by clouds, most climate models neglect cloud LW scattering to save computational costs. Ignoring cloud LW scattering directly overestimates outgoing longwave radiation (OLR). This study included ice-cloud LW scattering treatment in the Exascale Energy Earth System Model (E3SM) version 2 and ran fully-coupled simulations, prescribed sea surface temperature simulations, and offline radiative transfer calculations to comprehensively assess the impact of ice-cloud LW scattering on global climate simulation. The instantaneous effect due to ice-cloud LW scattering reduces the OLR by ~1 W/m^2 on the global average and 2 W/m^2 on the tropical average. Tropospheric warming and high cloud amount reduction act to partially compensate for such instantaneous OLR reduction caused by the inclusion of LW scattering. When the simulation reaches the equilibrium, the surface warms by 0.66 K on average with respect to the simulation without LW scattering, with the Arctic surface temperature differences more than twice as large as that of the global mean. The impact of including LW scattering on the simulated climate change in response to $4\times CO_2$ is also assessed. While including the cloud LW scattering does not significantly modify radiative forcing and total radiative feedback under such a scenario, it results in a 10% more positive cloud feedback.

Plain Language Summary

Clouds are an essential mediator in the climate system because they can reflect solar radiation back to space and block longwave radiation emitted below reaching the top of the atmosphere by either absorbing it or scattering it elsewhere. Such longwave scattering physics is deemed less important and thus neglected in most climate models to save computational time. We incorporated this mechanism into a climate model and ran pairs of simulations, with or without cloud scattering, to see how it would affect the simulated global climate. We found that cloud longwave scattering reduces the longwave radiation that goes to space. Such reduction of outgoing longwave radiation is strongest in the tropics. Compared to the simulation without longwave scattering, the mean-state surface temperature change is larger in the Arctic than in the tropics, which is primarily caused by the slow response to the inclusion of scattering. We also assessed to what extent the inclusion of cloud longwave scattering can affect the simulated response to abrupt $4\times CO_2$ increase. We concluded that it can increase the cloud feedback strength by ~10%, but overall, the impact is not statistically significant.

1. Introduction

Clouds play an important role in the climate system (Stephens, 2005; and references therein). Despite its importance in the climate system, cloud feedbacks still remain the largest uncertainty in climate feedback estimation (Sherwood et al., 2020). This is partly due to the multi-scale complexity of cloud processes, its intricate connections with large-scale dynamics, radiation, and cloud microphysics, and the oversimplification or exclusion of known physical processes by the climate models due to various computational constraints.

Cloud longwave (LW) scattering is one of such oversimplified or excluded physical processes in climate models. The cloud scattering effect is believed to be secondary in the LW due to strong absorption by greenhouse gases and clouds. As a result, the majority of climate models neglect LW scattering to save computational costs (Chen et al., 2020; Kuo et al., 2020). Earlier studies used offline radiative transfer calculation to show that omitting cloud LW scattering can lead to an overestimation of outgoing longwave radiation (OLR) (Stephens, 1980). Photons scattered by clouds will take a longer path to reach the top of the atmosphere (TOA), increasing the probability of being absorbed by greenhouse gas molecules, cloud particles, or the surface. This can further lead to a different atmospheric radiative cooling rate and a different surface downward LW flux (FLDS) (Ritter & Geleyn, 1992). Several parameterization schemes have been proposed to include multiple scattering of LW fluxes by clouds in climate models (Chou et al., 1999; Fu et al., 1997; Li & Fu, 2000). Using atmospheric profiles from model simulations or reanalysis, these studies estimated that when cirrus LW scattering is included, the instantaneous OLR can be reduced by

6~8 W/m^2 under the overcast conditions, and the FLDS can be increased by 2~4 W/m^2 correspondingly. (Chou et al., 1999; Fu et al., 1997; Joseph & Min, 2003; Ritter & Geleyn, 1992). Aside from cirrus clouds, which were believed to induce the most prominent LW scattering effect, some studies also highlighted the importance of scattered LW fluxes for radiation budget over the marine stratocumulus cloud regions (Costa & Shine, 2006; Kuo et al., 2017; Schmidt et al., 2006). It was estimated that, without LW scattering, the global mean OLR is overestimated by 1.5~3 W/m^2 (Costa & Shine, 2006; Kuo et al., 2017).

Beyond estimating the direct impact of cloud LW scattering on the radiation budget, efforts have been made to include cloud LW scattering in climate models to investigate how this can affect the overall simulated climate (Jin et al., 2019; Zhao et al., 2018). By examining prescribed sea surface temperature (SST) simulations, they estimated a global-mean OLR reduction by ~2.6 W/m^2 when the effect of cloud LW scattering is considered, which is 0.8 W/m^2 larger than the estimated instantaneous effect. Zhao et al. (2018) attributed it to the water vapor increase in response to the warming atmosphere. However, such prescribed-SST simulations cannot evaluate the impact of cloud LW scattering on surface climate as the surface-atmosphere coupling is constrained. To address this, Chen et al. (2020) used the Community Earth System Model (CESM) 1.1 slab-ocean model with a modified LW scheme to study the ice cloud LW scattering effect. They argued that cloud LW scattering is especially important over polar regions due to the small amount of water vapor in such regions. Their simulations showed a 1.0~2.0 K increase in the seasonal-mean surface air temperature over the polar region, which is at least twice as much as the increase in the tropics.

99 Such temperature increases in the polar regions are mostly absent in their prescribed-SST
100 simulations, highlighting the importance of surface-atmosphere coupling when evaluating the
101 impact of cloud LW scattering on simulated climate. However, the analysis by Chen et al. (2020)
102 is largely confined to the polar region without examining possible connections between extra-polar
103 and polar regions (Holland & Bitz, 2003; Stuecker et al., 2018).

104 To the best of our knowledge, no study has run fully-coupled simulations to assess the effect of
105 cloud LW scattering on the simulated climate. Unlike the slab-ocean models that do not include
106 ocean dynamics and prescribe the meridional heat transport by oceans, the fully-coupled models
107 have full ocean dynamics. They thus can represent the ocean's responses better. With these
108 simulations, we can analyze the fast adjustment (i.e., atmospheric and land processes when SST is
109 fixed) and slow adjustment (i.e., when SST is allowed to change) in response to the initial TOA
110 flux change caused by cloud LW scattering. Previous modeling studies have also limited their
111 scope to the mean state climate difference after including cloud LW scattering. Modification of
112 cloud optics could affect how the climate system responds to the increase of greenhouse gases. In
113 this study, we incorporate the same ice-cloud LW scattering treatment in Chen et al. (2020) into
114 the Exascale Energy Earth System Model (E3SM) version 2, a flagship climate model developed
115 by the Department of Energy (Golaz et al., 2022). Note that LW scattering by liquid water clouds
116 is not included here to be consistent with the treatment in Chen et al. (2020). The OLR reduction
117 caused by liquid cloud LW scattering is only ~1/2 of the reduction caused by ice cloud LW
118 scattering, although the FLDS increase caused by them is comparable (Kuo et al., 2017). This

119 study focuses on understanding the impact of ice cloud LW scattering, which also includes the LW
120 scattering of the ice portion of mixed-phase clouds. Hereafter, cloud LW scattering refers to ice
121 cloud LW scattering only. Using the modified model, we ran fully coupled simulations and
122 prescribed-SST simulations with cloud LW scattering on and off to evaluate how the inclusion of
123 cloud LW scattering can affect the simulated mean-state climate. The central question to answer
124 is that, for a climate model without scattering, how the fast process (i.e., direct atmospheric
125 responses) and slow processes respond to the inclusion of LW scattering to attain a new mean state.
126 Moreover, we ran additional pairs of $4\times CO_2$ simulations, with LW scattering on and off, to
127 investigate how enabling cloud LW scattering affects the simulated radiative feedback and climate
128 sensitivity.

129 Section 2 describes the model we used, our modifications, and the details of the numerical
130 experiments. After a brief analysis of the total mean-climate state change when cloud LW
131 scattering is included in section 3, section 4 delineates the instantaneous effect due to the inclusion
132 of cloud LW scattering, the fast response to such instantaneous effect, and the relationship between
133 them. The impact on radiative feedback and long-term surface temperature change, as seen in the
134 suites of $4\times CO_2$ experiments, is investigated in section 5, followed by a conclusion and discussion
135 section.

136 ## 2. Model, Data and Methods

137 ### 2.1. E3SM version 2

E3SMv2 (Golaz et al., 2022) is the successor of the first version of the E3SM model (E3SMv1) developed by the Department of Energy (Golaz et al., 2019). Although the first version was initially branched from CESM1, the second one is different from CESM as many components have been replaced or heavily modified, including the atmosphere dynamical core, ocean model, sea ice model, and river routing. Atmospheric physics in E3SMv2 still shares similarities with CESM2. To evaluate the model, the E3SM team conducted experiments according to a standard set of the Coupled Model Intercomparison Project Phase 6 (CMIP6) Diagnosis, Evaluation, and Characterization of Klima (DECK) simulations (Eyring et al., 2016). Compared to its predecessor, E3SMv2 doubles its speed and alleviates some issues. For example, it simulates better clouds and precipitation climatology and, consequently, improves the estimates of cloud feedbacks and equilibrium climate sensitivity (ECS). While E3SMv1 estimates an ECS of 5.3 K, which is deemed too high, E3SMv2 estimates a more realistic ECS value of 4.0 K (Golaz et al., 2022).

Our new fully-coupled simulations were branched from year 101 of the 500-year E3SMv2 pre-industrial control run (v2.LR.piControl), one of the standard runs in the CMIP6 DECK experiment. These simulations run on a horizontal grid of ~100 km in the atmosphere and land components, ½ degree in the river component, and 60 to 30 km in the ocean and sea-ice components. The atmosphere has 72 vertical layers from the surface to approximately 60 km. Note that the model runs on separate dynamics and column parameterization grids to improve computational efficiency. As a result, the dynamics grid has an average horizontal grid of 110 km, while the parameterization grid and the land grid have an average grid size of 165 km.

2.2. Model modifications to enable ice-cloud LW scattering

This study employed the same ice-cloud optics and longwave radiation schemes as described in Chen et al. (2020). In brief, a hybrid two-stream and four-stream (2S/4S) radiative transfer solver is implemented into the LW radiation scheme to enable cloud LW scattering. Compared to other solvers, the hybrid 2S/4S solver has a better compromise between accuracy and computational efficiency (Fu et al., 1997). The default ice-cloud optics in the E3SMv2 do not include ice-cloud scattering properties in the LW. In this study, cloud optical properties, including cloud extinction coefficients, single-scattering albedo, and asymmetry factors, are based on a cloud habit model (Yang et al., 2018) consistent with that used for the Moderate Resolution Imaging Spectroradiometer (MODIS) Collection 6 operational cloud products (Platnick et al., 2015; 2017). When cloud LW scattering is disabled, the extinction coefficient is set equal to the absorption coefficient. Details about the LW radiative transfer solver and ice-cloud optics can be found in Kuo et al. (2020) and Chen et al. (2020).

2.3. Numerical experiment design and data analysis

The scheme described in the previous subsection has been ported to the E3SMv2. We carried out four fully-coupled simulations, each one consisting of 105 years (i.e., year 0101 ~ 0205):

- Control: fully-coupled simulation without cloud LW scattering;
- Scat: fully-coupled simulation with cloud LW scattering;
- Control_4xCO2: same as Control, but the CO_2 concentration is set to four times of the piControl value, i.e., instantaneous quadrupling CO_2 experiment.

- Scat_4xCO2: same as Scat, but the CO_2 concentration is set to four times of the piControl value.

The other specifications of the four simulations are identical. By comparing the Scat case and the Control case, we can study the effects of cloud LW scattering on the simulated mean climate. With $4\times CO_2$ cases, we can further contrast climate feedbacks when cloud LW scattering is enabled or disabled. Note that the Control run is not the same as the standard E3SMv2 piControl run because the default ice-cloud optics are replaced with MODIS Collection 6 ice optics, and the radiative transfer solver is replaced by the hybrid 2S/4S solver with the LW scattering capability.

Figure 1 shows the time series of global-mean net TOA radiative flux imbalance and surface temperature of the four simulations. Because we replaced the ice-cloud optics and the radiative transfer solver, the Control run has a small TOA energy loss after branching from the equilibrated piControl run. Long-term mean TOA energy imbalance is -0.19 W/m^2. The Scat case, on the other hand, is closer to the equilibrium state (-0.01 W/m^2). The difference in surface temperature between the Scat and the Control case accumulates to ~0.6 K after about 30 years. Both Control_4xCO2 and Scat_4xCO2 have more than 1 W/m^2 net TOA energy imbalance throughout the simulations. However, the surface temperature in both cases becomes stable after about 70 years. For the last 30 years (year 0176 ~ 0205), the absolute trend of net TOA energy imbalance in all simulations is less than 0.02 W/m^2 per year, and the absolute trend of surface temperature is within 0.01 K per year. Therefore, we used the last 30 years of those simulations in all climatology

197 calculations in the following sections. Note that the difference in global-mean surface temperature
198 (Fig. 1b) between Scat and Control is similar to that between Scat_4xCO2 and Control_4xCO2.

199 3. Impact on Mean State Climate

200 3.1. Total Response in Equilibrium

201 Compared to a simulated climate system without LW scattering, the instantaneous effect of LW
202 scattering is to reduce the global-mean OLR (Costa & Shine, 2006; Kuo et al., 2017). Therefore,
203 more energy would be retained in the climate system and a warming climate can be expected.

204 Figure 2 summarizes the impacts on the surface climatology due to cloud LW scattering, where
205 the differences in global mean surface air temperature and downward longwave flux at surface
206 (FLDS) are plotted in each row. Panels (b) and (d) show the zonal mean differences of the
207 corresponding variables. In addition to the annual mean value (black), these panels also show the
208 changes in boreal summers (red) and boreal winters (blue). Globally speaking, the cloud LW
209 scattering effect results in a warmer surface by 0.66 K on average. The largest warming occurs in
210 the Arctic, where the annual-mean maximum exceeds 2 K. It is amplified in winters (~4 K) and
211 damped in summers (~0.5 K). Such seasonal variation is a typical feature of the polar amplification
212 phenomenon and can be explained by feedback processes in the Arctic region (Stuecker et al.,
213 2018; Boeke et al., 2021). Correspondingly, FLDS increases by approximately 4 W/m^2 on global
214 average. Its high correlation with surface air temperature is also consistent with what Chen et al.
215 (2020) has revealed.

Figure 3(a-c) shows the vertical temperature profile difference when the cloud LW scattering effect is enabled. For pure comparison purpose, the differences caused by the $4\times CO_2$ effect are also presented in Figure 3(d-f). Please note Figure 3(a-c) is the mean-state difference caused by including a physical process in the model while Figure 3(d-f) is the difference caused by abrupt $4\times CO_2$ increases in the original model without LW scattering. Regardless of the scale difference (2 K versus 20 K), they share some common features including the large warming of the upper troposphere in the tropics (Manabe & Wetherald, 1975; Manabe & Stouffer, 1980) and the confined near-surface warming in the Arctic. However, when cloud LW scattering is activated, the stratosphere does not cool as much as the one in the case of $4\times CO_2$ concentration. This can be explained by the fact that CO_2 has a strong stratospheric radiative cooling effect and, thus, increase of CO_2 directly affect the radiative equilibrium in the stratosphere; but enabling cloud longwave scattering would not directly affect the radiative cooling in the stratosphere.

3.2. Instantaneous Radiative Effect and Fast Response

Analogous to the concepts in radiative forcing and feedback analysis, in this section, we decomposed the total TOA flux changes (i.e., *total response*) due to the inclusion of cloud LW scattering into three parts: *instantaneous radiative effect* (analogous to IRF, instantaneous radiative forcing), *fast adjustment* (corresponding to rapid adjustment), and *slow adjustment*. The sum of the first two parts is termed the *fast response* (analogous to ERF, effective radiative forcing). We also decomposed FLDS into the same three parts to attribute the FLDS increase to physical processes.

236 The instantaneous radiative effect is defined as the radiative flux change when we only include the
237 cloud LW scattering physics; all atmospheric and surface state variables are fixed. In this case,
238 shortwave flux is unmodified. Similar to the approach in Zhao et al. (2018) to quantitatively derive
239 the scattered LW flux by clouds, we ran a short 3-year simulation configured similar to the Scat
240 case. While these runs evolve with cloud LW scattering enabled, the model outputs additional
241 longwave radiative fluxes and longwave heating rates computed in parallel but without the cloud
242 LW scattering effect. The instantaneous radiative effect is the difference between these extra
243 outputs (without scattering) and the original flux outputs (with scattering). Over the course of three
244 years, this difference shows a small seasonal variation (~1 W/m^2 for OLR and ~0.2 W/m^2 for FLDS)
245 and an even smaller annual variation (Figure S1). Hence, we think this derived instantaneous
246 radiative effect is applicable to interpret our fully-coupled simulation results.

247 Figure 4 shows the zonal mean instantaneous OLR change and FLDS change, as well as the total
248 response, due to the cloud LW scattering effect. Here, cloud LW scattering reduces the OLR by
249 1.13 W/m^2 globally on average. The largest decrease is seen in the tropics by 2 W/m^2, while the
250 smallest decrease occurs in the polar region and the subtropical region (<1 W/m^2). Such latitudinal
251 distribution is consistent with Kuo et al. (2017) and Costa & Shine (2006). Note that the
252 instantaneous FLDS increase due to the scattered LW flux by ice clouds is only 0.08 Wm^{-2}, only
253 ~2% of the FLDS increase for the total response (3.95 W/m^2 globally), suggesting that climate
254 feedbacks must play an important role in the change of FLDS.

255 Fast response here is defined as the TOA flux changes when SST and sea ice conditions are fixed.
256 This is equal to the instantaneous radiative effect plus the fast adjustment due to changes in
257 atmospheric temperature, land temperature, water vapor concentration, and clouds. To derive this
258 quantity, we ran two 35-year prescribed-SST simulations, one with cloud LW scattering and one
259 without. Only the atmosphere component is active, while SST and sea ice are prescribed using
260 historical observations from 1980 to 2014. The zonal mean OLR and FLDS differences between
261 these two runs are plotted as blue curves in Figure 4. We also calculated the contributions to the
262 flux changes from individual components of the atmosphere-surface system using a radiative
263 kernel (Huang et al., 2017) except clouds. Cloud adjustments are directly calculated from all-sky
264 and clear-sky fluxes output from the model. The impact on the TOA fluxes is summarized in Table
265 1.

266 Following the instantaneous OLR reduction due to the LW scattering effect, fast adjustments
267 increase the OLR by 0.44 W/m^2. The sum of individual fast adjustment terms is 0.45 W/m^2, close
268 to the amount above, which confirms the validity of using a radiative kernel to decompose the fast
269 adjustment. Major contributors to the OLR increase include cloud LW radiative effect (0.283
270 W/m^2), tropospheric warming (0.260 W/m^2), and land surface warming (0.028 W/m^2).
271 Stratospheric temperature change only leads to a small change in OLR by -0.013 W/m^2. This
272 phenomenon is a typical feature of increased absorption in the troposphere but nearly unchanged
273 absorption in the stratosphere, as this is comparable to the pattern of the rapid adjustment when
274 black carbon is injected into the troposphere (Smith et al., 2018). Consequently, the TOA flux

imbalance becomes smaller, and the peak in the tropics is also shaved (Figure 4a). The FLDS change after fast adjustments increases by 0.35 W/m^2, primarily due to tropospheric warming (Figure 4b). The increase in the Arctic is larger than the global mean (~1 W/m^2).

As for the slow adjustment to further compensate for the TOA flux imbalance of 0.67 W/m^2 (the imbalance caused by the instantaneous effect of the inclusion of cloud LW scattering and the fast response to such inclusion together), it consists of the surface temperature increase and the subsequent state variable changes via various feedback mechanisms. As a result, the global-mean OLR in the Scat case now exceeds the one in the Control case (Figure 4a) and the global-mean shortwave flux in the Scat case is smaller than it in the control case (thus the net TOA imbalance becomes closer to zero). Ultimately, cloud LW scattering induces a small warming effect globally. The ratio of net TOA flux changes and surface temperature increase (0.66 K) in the slow process is approximately -0.9 $W/m^2/K$, a value that is close to the one in the case of CO_2 concentration increase (which will be discussed in the next section). Driven by surface warming, FLDS in total response is significantly stronger, especially in the Arctic where the magnitude exceeds 10 W/m^2 (Figure 4b). This suggests that the large increase of FLDS in the Arctic is dominantly caused by the slow adjustment. Because of the positive correlation between FLDS and TS, it can be inferred that the strong warming in the Arctic region should be attributed to the slow adjustments instead of the instantaneous radiative effect. Total responses seen in cloud fraction and properties are also the consequence of slow adjustments, including ice-to-liquid transition in tropical mid-troposphere (Figure S2), elevated deep convective clouds (Figure S3), reduced anvil cloud coverage (Figure

S3), and increased stratiform low cloud coverage (Figure S4).

4. Impact on the Simulated Climate Change Under 4×CO_2 Scenario

In addition to the impact on the simulated mean-state climatology, a more scientifically intriguing question is to what extent the inclusion of cloud LW scattering can affect the simulated climate change in response to the increase of greenhouse gases. This section discusses this effect in the context of abrupt 4×CO_2 simulations.

We adopted the regression approach to calculate the ERF and total climate feedback for the cases with or without cloud LW scattering (Gregory et al., 2004). Figure 5 shows the scatterplot of annual-mean net TOA radiation with respect to surface temperature (a.k.a., Gregory plot) for both cases. The scatter points for both Control and Scat cases mix with each other. While the inclusion of cloud LW scattering tends to decrease the ERF and increase the total feedback, the differences are statistically negligible: the slopes of two corresponding regression lines (i.e., Control and Scat) only differ by 0.03 W/m^2/K, with a large overlap between their 95% confidence intervals (i.e., -0.74±0.08 vs -0.71±0.09 W/m^2/K); the intercept difference is 0.24 W/m^2, also with a large overlap between their 95% confidence intervals (i.e., 6.28±0.49 vs 6.04±0.54) W/m^2. Thus, two regression results are statistically indistinguishable. Consistent with such assessment, the global-mean surface temperature changes due to 4×CO_2, as inferred from the last 30 years of simulations (Figure 1), are 6.8 K for the Control case and 6.7 K for the Scat case, also suggesting that the cloud LW scattering affects little on such climate projection simulation.

To gain a detailed understanding of how the LW scattering affects individual radiative feedback strength, we decompose the total feedback into different components using the radiative kernel approach. We employed the same radiative kernel used in Section 4 to derive Planck feedback, lapse rate feedback, water vapor feedback, and surface albedo feedback. Cloud feedbacks are calculated using cloud radiative kernels similar to Zelinka et al. (2012a; 2012b). As the kernel in Zelinka et al. (2012a, 2012b) was built without LW cloud scattering, we calculated a correction term based on offline radiative transfer calculations with LW scattering turning on and off, and derive two sets of LW cloud radiative kernels using the approach described in Zelinka et al. (2012a). Then, we took the difference between the two kernels and deemed it as the correction term to the original Zelinka's LW cloud radiative kernel. Figure 6a visualizes the kernel without cloud LW scattering, and figure 6b shows the correction term. The correction term can exceed 10% for high cloud with optical depth ≤ 3.6.

Figure 7 summarizes the decomposition of the total radiative feedback into individual terms. Two sets of cloud feedback are included using the original cloud radiative kernel and the new kernel with the correction term. Accounting for the correction due to cloud LW scattering, the largest absolute change in individual terms is the cloud feedback. Both LW and SW parts contribute to the increase in cloud feedback, together adding ~10% of the total cloud feedback strength to the counterpart derived from the Control simulations (i.e., without cloud LW scattering). Lapse rate feedback and water vapor feedback are also modified when cloud LW scattering is included, but these changes almost cancel out. Surface albedo feedback also decreases by approximately 0.03

334 $W/m^2/K$, or 6% of that in the Control case. With the correction term, the sum of changes from each
335 individual term has a much better agreement with the change in total feedback strength estimated
336 from the regression method (lower right panel in Fig. 7). Nevertheless, given the uncertainty of
337 climate feedback estimation and because the ice cloud LW scattering effect on feedback terms is
338 small in magnitude, few differences shown in Fig. 7 are likely to be statistically significant.

339 ## 5. Conclusions

340 We modified the E3SM version 2, a fully-coupled climate model, to include the ice cloud LW
341 scattering effect, a physical process omitted by most climate models. Based on the modified model,
342 we ran simulations with our modifications enabled and disabled to study the impact of ice cloud
343 LW scattering on the simulated climate system, for both the mean-state and climate-change
344 simulations. Figure 8 summarizes the radiative and temperature responses to the inclusion of ice
345 cloud LW scattering.

346 Compared to the simulation without longwave scattering, the instantaneous radiative effect due to
347 ice cloud LW scattering reduces the OLR (outgoing longwave radiation) across all latitudes. The
348 strongest OLR reduction occurs in the tropics. Most scattered fluxes are absorbed in the
349 atmosphere instead of reflected to the surface, as the instantaneous increase of FLDS (downward
350 longwave radiative flux at the surface) is negligible compared to the OLR reduction. The OLR
351 reduction is compensated to some extent, primarily by the warming troposphere and cloud LW
352 effect through fast adjustments. Stratosphere contributes little here as the LW scattering alters the
353 radiative flux throughout the troposphere but has little effect on the stratosphere. The majority of

the total FLDS increase, as well as the highly correlated surface temperature increase, is primarily due to the slow adjustment. Consequently, compared to the mean-state climate simulated by the model without LW scattering, the global-mean surface temperature difference is +0.66 K, with the difference in the Arctic at least twice as much as the global mean difference, especially in boreal winter.

In the scenario of abrupt $4\times CO_2$ simulations, ice cloud LW scattering does not significantly modify ERF (effective radiative forcing) and climate feedbacks. The ERF and total feedback strengths inferred from two pairs of simulations, with and without ice cloud LW scattering, has no statistically significant differences. When total feedback is decomposed to individual feedback using the radiative kernel technique, the most notable change is the 10% increase of cloud feedback due to the inclusion of ice cloud LW scattering. Such a change might not be statistically significant, though, given the uncertainty of cloud feedback.

This study refines and deepens our understanding of the cloud LW scattering effect. The explanation in Chen et al. (2020) for the simulated responses of mean states in the polar region overlooked the global connections, especially the changes in the tropics caused by cloud LW scattering. We took advantage of fully-coupled simulations, prescribed simulations, and offline radiative transfer calculations to analyze the instantaneous effect, fast adjustment, and slow adjustment after including the scattering physics. These analyses delineate a full picture of how the inclusion of cloud LW scattering affects the simulation of the mean-state climate. This study revealed that the strong response in the Arctic is primarily due to the highly sensitive nature of the

polar climate. The instantaneous OLR reduction due to cloud LW scattering is indeed relatively weak in the Arctic. In addition, we assessed how including cloud LW scattering physics can affect ERF and climate feedbacks caused by the increase of CO_2. While the impacts on the ERF and climate feedbacks are statistically insignificant, the cloud LW scattering is more inclined to increase the total feedback via more positive cloud feedback. Note that liquid cloud LW scattering is not studied here. Considering the different spatial distributions of ice clouds and liquid clouds, liquid cloud LW scattering effect may have different structural impacts on mean-state climate and climate feedback. Future work is warranted to assess the impact of liquid cloud LW scattering on climate simulations.

Cloud LW scattering is one example of physical processes that are often neglected in climate modeling studies. A variety of compensating biases occur in any fully-coupled climate model simulations. The inclusion of cloud LW scattering reduce one type of structural uncertainties in the climate models. While such reduction of structural uncertainties might not directly lead to an improved climate simulations (as the modified model might needs to be re-tuned), it could help expose other compensating errors. Future work is warranted to compare the historical runs based on this modified model to satellite observations and reanalysis products. It can also be beneficial in future studies to include cloud LW scattering in other climate models and assess the impact on multi-model mean state as well as individual model simulation. In terms of computational costs, the modifications cost 10% additional computational time compared to the original E3SMv2 model.

Because of the three-dimensional nature of scattering, it would be a meaningful follow-up study to examine the cloud LW scattering effect in the context of 3D radiative transfer (e.g., Kablick et al., 2011), especially for high-spatial-resolution global simulations such as those global storm-resolving models with a spatial resolution as high as 1~3 km (Stevens et al., 2019). The horizontal photon flux transport, which is entirely neglected in plane-parallel radiative transfer calculation, could become important for certain cloud regimes (e.g., cumulus and stratocumulus) in such global storm-resolving model simulations.

Acknowledgment

We thank the Editor, the Associate Editor, and three reviewers for their constructive and insightful comments, which greatly increase the clarity and intellectual value of this study. This material is based upon work supported by the U.S. Department of Energy, Office of Science, Office of Biological and Environmental Research, Climate and Environmental Science Division under Awards DE-SC0019278 and DE-SC0022117 to the University of Michigan with a subcontract to Texas A&M. YHC performed relevant work for this project entirely during his stay at the University of Michigan. We wish to thank Dr. Xianwen Jing for his contribution to code development during his postdoctoral stay at the University of Michigan. CXF also acknowledges the support from the NASA FINNEST program under Grant No. 80NSSC22K1433 for part of the studies presented here.

Open Research

The source code of the original E3SM version 2 can be found in a publicly accessible repository (E3SM Project, 2021; Golaz et al., 2022). The source code of our modified model is currently preserved on Zenodo (Fan et al., 2023). The Control run can be reproduced using the cxfan/v2.LR.piControl.0101.UMRad.CTRL branch, and the Scat run using the cxfan/v2.LR.piControl.0101.UMRad.Scat branch. Model outputs were processed using netCDF Operator (NCO; Zender, 2022) and xarray v2023.02.0 (Hoyer & Hamman, 2017; Hoyer et al., 2023). The radiative kernel used to decompose individual feedback terms can be downloaded from Mendeley Data archive (Huang, 2022; Huang et al., 2017). Figures were produced with Matplotlib version 3.6.3 (Caswell et al., 2020; Hunter, 2007).

References

Boeke, R. C., Taylor, P. C., & Sejas, S. A. (2021). On the Nature of the Arctic's Positive Lapse-Rate Feedback. *Geophysical Research Letters*, *48*(1). https://doi.org/10.1029/2020gl091109

Bony, S., Stevens, B., Coppin, D., Becker, T., Reed, K. A., Voigt, A., & Medeiros, B. (2016). Thermodynamic control of anvil cloud amount. *Proceedings of the National Academy of Sciences*, *113*(32), 8927–8932. https://doi.org/10.1073/pnas.1601472113

Caswell, T. A., Lee, A., Droettboom, M., Andrade, E. S., Hoffmann, T., Klymak, J., et al. (2020). matplotlib/matplotlib: REL: v3.6.3 [Software]. Zenodo. https://doi.org/10.5281/zenodo.7527665

Chen, Y., Huang, X., Yang, P., Kuo, C., & Chen, X. (2020). Seasonal Dependent Impact of Ice Cloud Longwave Scattering on the Polar Climate. *Geophysical Research Letters*, *47*(23). https://doi.org/10.1029/2020gl090534

Chou, M.-D., Lee, K.-T., Tsay, S.-C., & Fu, Q. (1999). Parameterization for Cloud Longwave Scattering for Use in Atmospheric Models. *Journal of Climate*, *12*(1), 159–169. https://doi.org/10.1175/1520-0442(1999)012<0159:pfclsf>2.0.co;2

Costa, S. M. S., & Shine, K. P. (2006). An estimate of the global impact of multiple scattering by clouds on outgoing long-wave radiation. *Quarterly Journal of the Royal Meteorological Society*, *132*(616), 885–895. https://doi.org/10.1256/qj.05.169

E3SM Project, DOE. (2021). Energy Exascale Earth System Model v2.0. [Software]. https://doi.org/10.11578/E3SM/dc.20210927.1.

Eyring, V., Bony, S., Meehl, G. A., Senior, C. A., Stevens, B., Stouffer, R. J., & Taylor, K. E. (2016). Overview of the Coupled Model Intercomparison Project Phase 6 (CMIP6) experimental design and organization. *Geoscientific Model Development*, *9*(5), 1937–1958. https://doi.org/10.5194/gmd-9-1937-2016

Fan, C., Chen, Y.-H., Chen, X., Lin, W., Yang, P., Huang, X., et al. (2023). cxfan1997/E3SM: UMRad E3SMv2 First Release [Software]. Zenodo. https://doi.org/10.5281/zenodo.7916862

448 Fu, Q., Liou, K. N., Cribb, M. C., Charlock, T. P., & Grossman, A. (1997). Multiple Scattering
449 Parameterization in Thermal Infrared Radiative Transfer. *Journal of the Atmospheric*
450 *Sciences*, *54*(24), 2799–2812. https://doi.org/10.1175/1520-
451 0469(1997)054<2799:mspiti>2.0.co;2

452 Golaz, J.-C., Caldwell, P. M., Van Roekel, L. P., Petersen, M. R., Tang, Q., Wolfe, J. D., et al.
453 (2019). The DOE E3SM coupled model version 1: Overview and evaluation at standard
454 resolution. *Journal of Advances in Modeling Earth Systems, 11*, 2089–2129.
455 https://doi.org/10.1029/2018MS001603

456 Golaz, J.-C., Van Roekel, L. P., Zheng, X., Roberts, A. F., Wolfe, J. D., Lin, W., et al. (2022).
457 The DOE E3SM Model Version 2: Overview of the physical model and initial model
458 evaluation. *Journal of Advances in Modeling Earth Systems, 14*, e2022MS003156.
459 https://doi.org/10.1029/2022MS003156

460 Gregory, J. M., Ingram, W. J., Palmer, M. A., Jones, G. S., Stott, P. A., Thorpe, R. B., et al.
461 (2004). A new method for diagnosing radiative forcing and climate sensitivity. *Geophysical*
462 *Research Letters*, *31*(3), L03205. https://doi.org/10.1029/2003gl018747

463 Hartmann, D. L., & Short, D. A. (1980). On the Use of Earth Radiation Budget Statistics for
464 Studies of Clouds and Climate. *Journal of the Atmospheric Sciences*, *37*(6), 1233–1250.
465 https://doi.org/10.1175/1520-0469(1980)037<1233:otuoer>2.0.co;2

Hartmann, D. L. & Larson, K. (2002). An important constraint on tropical cloud - climate feedback. *Geophysical Research Letters, 29*, 1951. https://doi.org/10.1029/2002GL015835

Holland, M. M., & Bitz, C. M. (2003). Polar amplification of climate change in coupled models. *Climate Dynamics*, *21*, 221–232. https://doi.org/10.1007/s00382-003-0332-6

Hoyer, S. & Hamman, J., (2017). xarray: N-D labeled Arrays and Datasets in Python. *Journal of Open Research Software, 5*(1), 10. https://doi.org/10.5334/jors.148

Hoyer, S., Roos, M., Joseph, H., Magin, J., Cherian, D., Fitzgerald, C., et al. (2023). xarray (Version v2023.02.0) [Software]. Zenodo. https://doi.org/10.5281/zenodo.7616056

Huang, Y., Xia, Y., & Tan, X. (2017). On the pattern of CO2 radiative forcing and poleward energy transport. *Journal of Geophysical Research: Atmospheres*, *122*(20), 10,578-10,593. https://doi.org/10.1002/2017jd027221

Huang, Y. (2022). ERA-interim reanalysis based radiative kernels [Dataset], Mendeley Data. https://doi.org/10.17632/3drx8fmmz9.1

Hunter, J. D. (2007). Matplotlib: A 2D Graphics Environment. *Computing in Science & Engineering*, *9*(3), 90-95. https://doi.org/10.1109/MCSE.2007.55.

Jin, Z., Zhang, Y., Genio, A. D., Schmidt, G., & Kelley, M. (2019). Cloud scattering impact on thermal radiative transfer and global longwave radiation. *Journal of Quantitative*

Spectroscopy and Radiative Transfer, *239*, 106669. https://doi.org/10.1016/j.jqsrt.2019.106669

Joseph, E., & Min, Q. (2003). Assessment of multiple scattering and horizontal inhomogeneity in IR radiative transfer calculations of observed thin cirrus clouds. *Journal of Geophysical Research: Atmospheres*, *108*, 4380. https://doi.org/10.1029/2002jd002831

Kablick, G. P., Ellingson, R. G., Takara, E. E., & Gu, J. (2011). Longwave 3D Benchmarks for Inhomogeneous Clouds and Comparisons with Approximate Methods. *Journal of Climate 24*, 2192–2205. https://doi.org/10.1175/2010jcli3752.1

Klein, S.A., Hall, A., Norris, J.R., & Pincus, R. (2017). Low-Cloud Feedbacks from Cloud-Controlling Factors: A Review. *Surveys in Geophysics, 38*, 1307–1329. https://doi.org/10.1007/s10712-017-9433-3

Kuo, C., Yang, P., Huang, X., Feldman, D., Flanner, M., Kuo, C., & Mlawer, E. J. (2017). Impact of Multiple Scattering on Longwave Radiative Transfer Involving Clouds. *Journal of Advances in Modeling Earth Systems*, *9*(8), 3082–3098. https://doi.org/10.1002/2017ms001117

Kuo, C., Yang, P., Huang, X., Chen, Y.., & Liu, G. (2020). Assessing the accuracy and efficiency of longwave radiative transfer models involving scattering effect with cloud optical

property parameterizations. *Journal of Quantitative Spectroscopy and Radiative Transfer*, *240*, 106683. https://doi.org/10.1016/j.jqsrt.2019.106683

Li, J., & Fu, Q. (2000). Absorption Approximation with Scattering Effect for Infrared Radiation. *Journal of the Atmospheric Sciences*, *57*(17), 2905–2914. https://doi.org/10.1175/1520-0469(2000)057<2905:aawsef>2.0.co;2

Manabe, S., & Wetherald, R. T. (1975). The Effects of Doubling the CO2 Concentration on the climate of a General Circulation Model. *Journal of the Atmospheric Sciences, 32*(1), 3–15. https://doi.org/10.1175/1520-0469(1975)032<0003:teodtc>2.0.co;2

Manabe, S., & Stouffer, R. J. (1980). Sensitivity of a global climate model to an increase of CO2 concentration in the atmosphere. *Journal of Geophysical Research: Oceans, 85*(C10), 5529–5554. https://doi.org/10.1029/jc085ic10p05529

Mauritsen, T., & Stevens, B. (2015). Missing iris effect as a possible cause of muted hydrological change and high climate sensitivity in models. *Nature Geoscience*, *8*(5), 346–351. https://doi.org/10.1038/ngeo2414

McCoy, D. T., Eastman, R., Hartmann, D. L., & Wood, R. (2017). The Change in Low Cloud Cover in a Warmed Climate Inferred from AIRS, MODIS, and ERA-Interim. *Journal of Climate*, *30*(10), 3609–3620. https://doi.org/10.1175/jcli-d-15-0734.1

517 Platnick, S., Meyer, K. G., King, M. D., Wind, G., Amarasinghe, N., Marchant, B., et al. (2015).
518 *MODIS cloud optical properties: User guide for the collection 6 level-2 MOD06/MYD06*
519 *product and associated level-3 datasets, version 1.0*. Retrieved from http://modis-atmos.gsfc.
520 nasa.gov/_docs/C6MOD06OPUserGuide.pdf

521 Platnick, S., Meyer, K. G., King, M. D., Wind, G., Amarasinghe, N., Marchant, B., et al. (2017).
522 The MODIS Cloud Optical and Microphysical Products: Collection 6 Updates and Examples
523 from Terra and Aqua. *IEEE Transactions on Geoscience and Remote Sensing*, *55*(1), 502–
524 525. https://doi.org/10.1109/tgrs.2016.2610522

525 Qu, X., Hall, A., Klein, S. A., & Caldwell, P. M. (2014). On the spread of changes in marine low
526 cloud cover in climate model simulations of the 21st century. *Climate Dynamics*, *42*, 2603–
527 2626. https://doi.org/10.1007/s00382-013-1945-z

528 Ritter, B., & Geleyn, J.-F. (1992). A Comprehensive Radiation Scheme for Numerical Weather
529 Prediction Models with Potential Applications in Climate Simulations. *Monthly Weather*
530 *Review*, *120*(2), 303–325. https://doi.org/10.1175/1520-0493(1992)120<0303:acrsfn>2.0.co;2

531 Schmidt, G. A., Ruedy, R., Hansen, J. E., Aleinov, I., Bell, N., Bauer, M., et al. (2006). Present-
532 Day Atmospheric Simulations Using GISS ModelE: Comparison to In Situ, Satellite, and
533 Reanalysis Data. *Journal of Climate*, *19*(2), 153–192. https://doi.org/10.1175/jcli3612.1

Sherwood, S. C., Webb, M. J., Annan, J. D., Armour, K. C., Forster, P. M., Hargreaves, J. C., et al. (2020). An Assessment of Earth's Climate Sensitivity Using Multiple Lines of Evidence. *Reviews of Geophysics*, *58*(4), e2019RG000678. https://doi.org/10.1029/2019rg000678

Smith, C. J., Kramer, R. J., Myhre, G., Forster, P. M., Soden, B. J., Andrews, T., et al. (2018). Understanding Rapid Adjustments to Diverse Forcing Agents. *Geophysical Research Letters*, *45*(21), 12023–12031. https://doi.org/10.1029/2018gl079826

Stephens, G. L. (1980). Radiative Properties of Cirrus Clouds in the Infrared Region. *Journal of the Atmospheric Sciences*, *37*(2), 435–446. https://doi.org/10.1175/1520-0469(1980)037<0435:rpocci>2.0.co;2

Stephens, G. L. (2005). Cloud Feedbacks in the Climate System: A Critical Review. *Journal of Climate, 18*(2), 237–273. https://doi.org/10.1175/jcli-3243.1

Stevens, B., Satoh, M., Auger, L., Biercamp, J., Bretherton, C. S., Chen, X., et al. (2019). DYAMOND: the DYnamics of the Atmospheric general circulation Modeled On Non-hydrostatic Domains. *Progress in Earth and Planetary Science, 6*, 61. https://doi.org/10.1186/s40645-019-0304-z

Stuecker, M. F., Bitz, C. M., Armour, K. C., Proistosescu, C., Kang, S. M., Xie, S.-P., et al. (2018). Polar amplification dominated by local forcing and feedbacks. *Nature Climate Change*, *8*(12), 1076–1081. https://doi.org/10.1038/s41558-018-0339-y

552 Wood, R., & Bretherton, C. S. (2006). On the Relationship between Stratiform Low Cloud Cover
553 and Lower-Tropospheric Stability. *Journal of Climate*, *19*(24), 6425–6432.
554 https://doi.org/10.1175/jcli3988.1

555 Yang, P., S. Hioki, M. Saito, C.-P. Kuo, B. A. Baum, K.-N. Liou, 2018: A review of ice cloud
556 optical property models for satellite remote sensing, *Atmosphere, 9*, 499.
557 https://doi.org/10.3390/atmos9120499

558 Yoshimori, M., Lambert, F. H., Webb, M. J. & Andrews, T. (2020). Fixed anvil temperature
559 feedback - positive, zero or negative? *Journal of Climate, 33*, 2719–2739.
560 https://doi.org/10.1175/JCLI-D-19-0108.1

561 Zelinka, M. D., & Hartmann, D. L. (2010). Why is longwave cloud feedback positive? *Journal*
562 *of Geophysical Research: Atmospheres*, *115*, D16117. https://doi.org/10.1029/2010jd013817

563 Zelinka, M. D., & Hartmann, D. L. (2011). The observed sensitivity of high clouds to mean
564 surface temperature anomalies in the tropics. *Journal of Geophysical Research: Atmospheres*,
565 *116*, D23103. https://doi.org/10.1029/2011jd016459

566 Zelinka, M. D., Klein, S. A., & Hartmann, D. L. (2012a). Computing and Partitioning Cloud
567 Feedbacks Using Cloud Property Histograms. Part I: Cloud Radiative Kernels. *Journal of*
568 *Climate*, *25*(11), 3715–3735. https://doi.org/10.1175/jcli-d-11-00248.1

569 Zelinka, M. D., Klein, S. A., & Hartmann, D. L. (2012b). Computing and Partitioning Cloud
570 Feedbacks Using Cloud Property Histograms. Part II: Attribution to Changes in Cloud
571 Amount, Altitude, and Optical Depth. *Journal of Climate*, *25*(11), 3736–3754.
572 https://doi.org/10.1175/jcli-d-11-00249.1

573 Zender, C. S. (2022), netCDF Operator (NCO), Version 5.0.7 [Software].
574 https://nco.sourceforge.net/

575 Zhao, W., Peng, Y., Wang, B., & Li, J. (2018). Cloud Longwave Scattering Effect and Its Impact
576 on Climate Simulation. *Atmosphere*, *9*(4), 153. https://doi.org/10.3390/atmos9040153

577

Tables

Table 1. Simulated global-mean net radiative flux change at the TOA (unit of W/m^2, positive downward) due to the inclusion of cloud LW scattering. Wherever applicable, flux changes are separated into longwave and shortwave components. The instantaneous effect, fast response, and total response are shown, as well as their differences. Fast adjustment is decomposed into six terms using a radiative kernel. The sum of these individual terms is shown at the last row, which can be compared to the fast adjustment term at the fifth row.

	Longwave (W/m^2)	**Shortwave (W/m^2)**	**Total (W/m^2)**
Total Response	–0.606	0.717	0.111
Instantaneous Effect	1.127		1.127
Fast Response	0.670	0.023	0.692
Fast Adjustment (Fast Resp.– Instantaneous)	–0.457	0.023	–0.435
Slow Adjustment (Total Resp. – Fast Resp.)	–1.276	0.694	–0.581
Contribution to the fast adjustment from different factors			
Surface Temperature	–0.028		–0.028
Tropospheric Temperature	–0.260		–0.260
Stratospheric Temperature	0.013		0.013
Water Vapor	0.080	0.022	0.102
Surface Albedo		0.032	0.032
Cloud	–0.283	–0.021	–0.304
Sum of Individual Terms	–0.478	0.033	–0.445

Figures

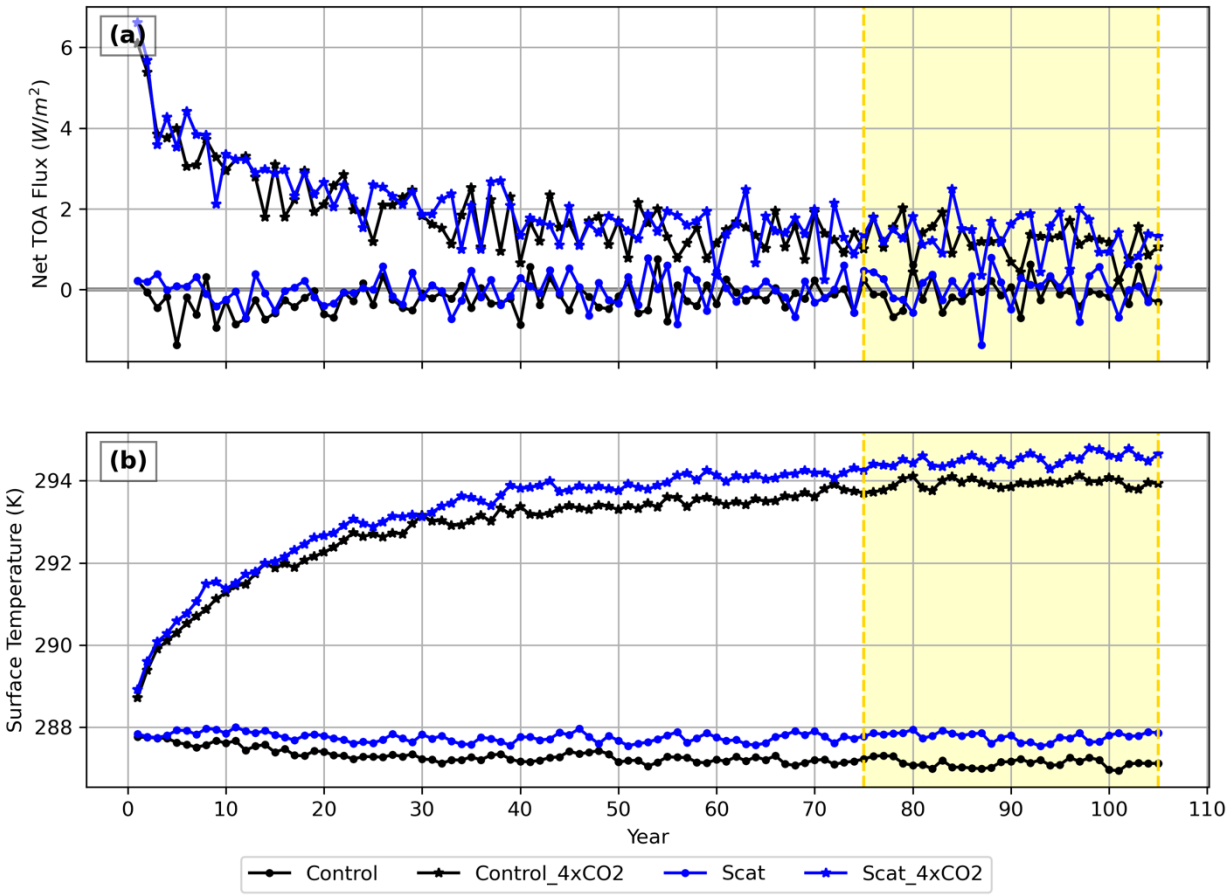

Figure 1. Annual-mean time series of (a) global mean energy imbalance at the top of the atmosphere (TOA), defined as net downward flux; and (b) global mean surface skin temperature. The Scat and Control cases are shown in blue and black, respectively. The cases under preindustrial control scenario are marked by dots, while the cases under $4\times CO_2$ scenario are marked by stars. The yellow highlighted region indicates the time period we used in all climatological calculations.

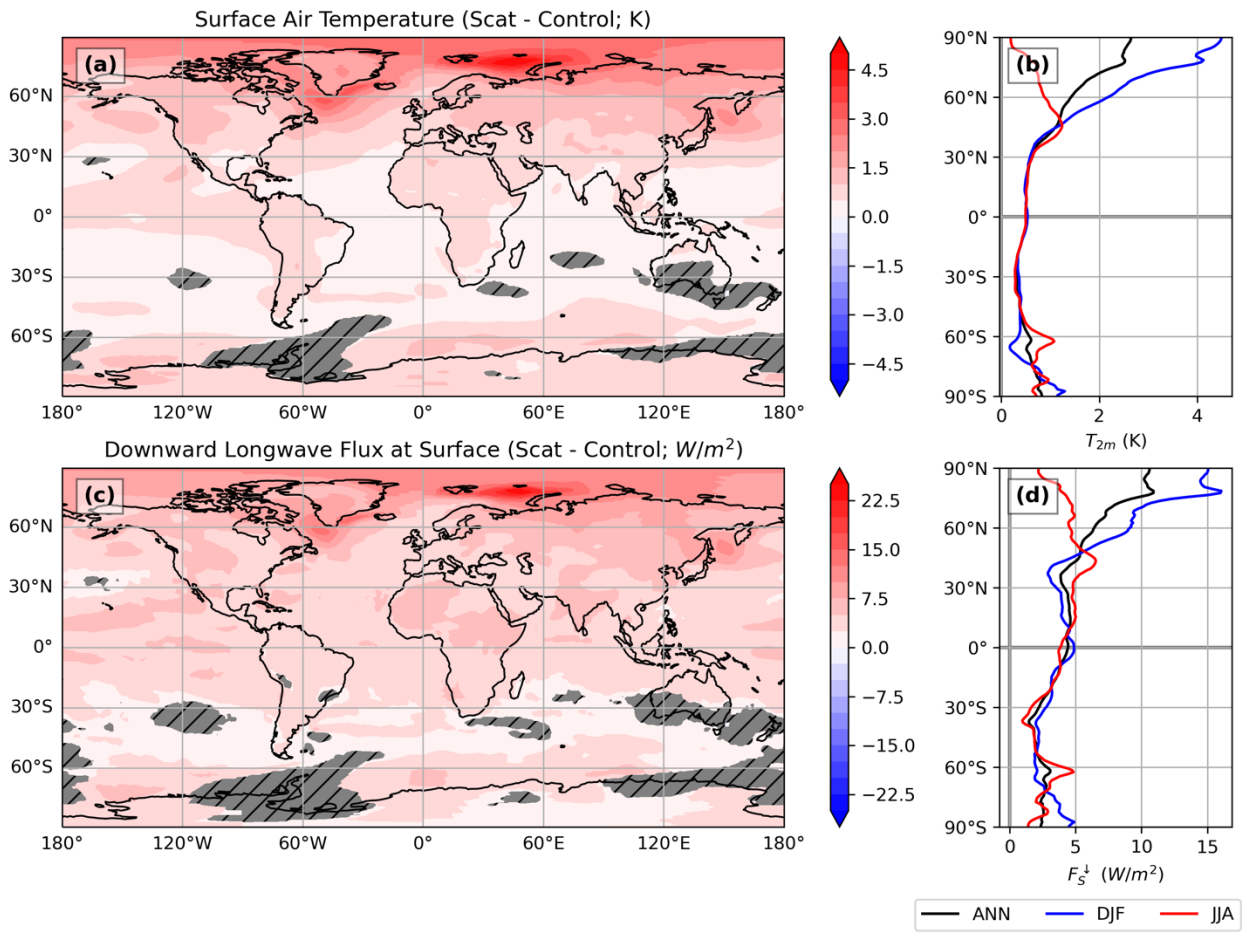

Figure 2. Comparison of the surface climatology between the Scat case and the Control case. (a) Annual-mean surface air temperature difference. (b) Zonal-mean surface air temperature difference in annual mean (black), boreal summer season (JJA; red), and boreal winter season (DJF; blue). (c,d) Same as (a,b) but for FLDS. Gray slat patches mask the region without statistically significant changes (1% significance level).

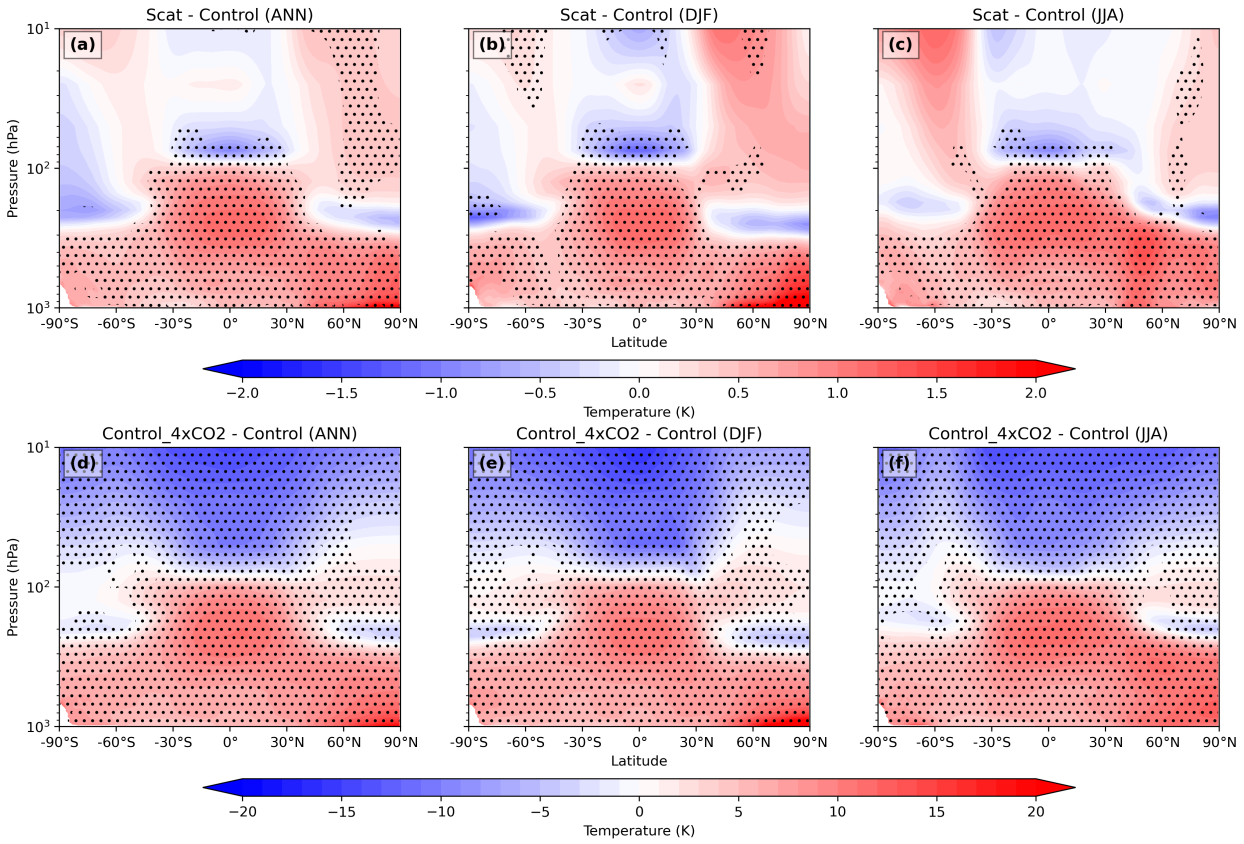

601

602 **Figure 3.** (a) Annual- and zonal-mean differences in vertical temperature profile resulting from
603 the cloud LW scattering effect; (b) the same zonal-mean difference but in boreal winter seasons
604 (DJF); (c) the same zonal-mean difference but in boreal summer seasons (JJA); (d-f) the same as
605 (a-c), but the contour shows the vertical temperature profile change due to abrupt $4\times CO_2$
606 concentration. Black dots indicate statistically significant temperature change at 1% significance
607 level.

608

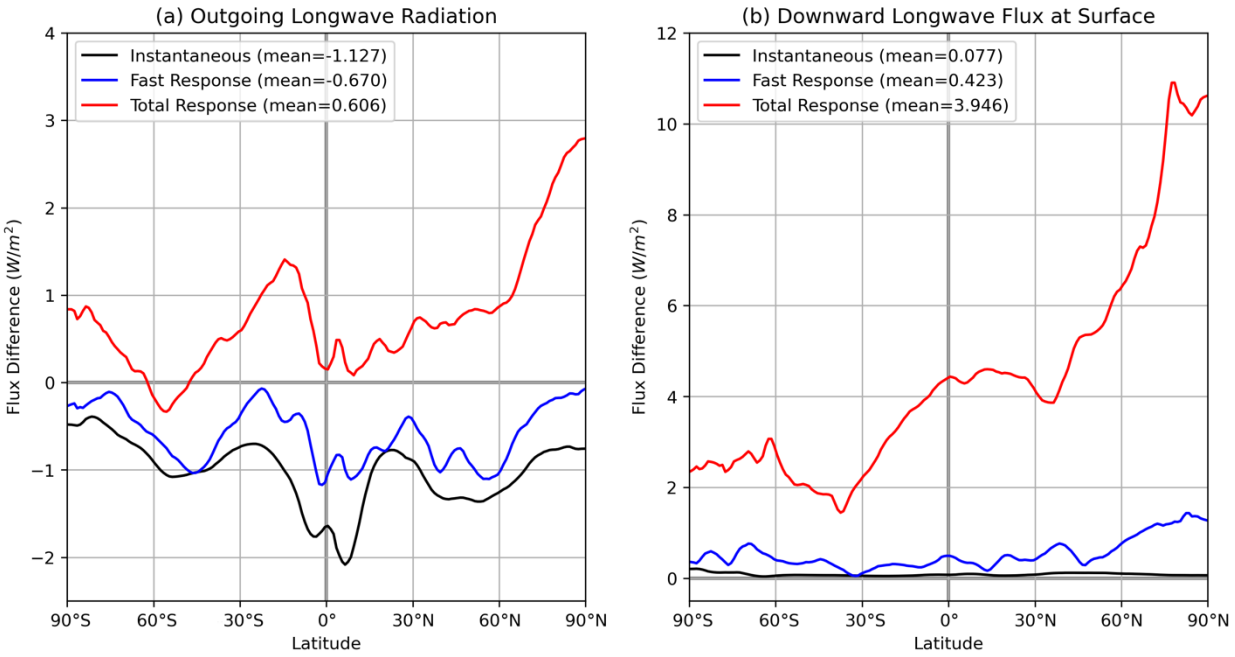

609

610 **Figure 4.** Zonal mean flux changes from instantaneous radiative effect (black), fast response (blue),
611 and total response (red) caused by the inclusion of cloud LW scattering. (a) outgoing longwave
612 radiation, where net upward is positive; (b) downward longwave flux at surface, where net
613 downward is positive. The global average of each component is indicated in the legend.

614

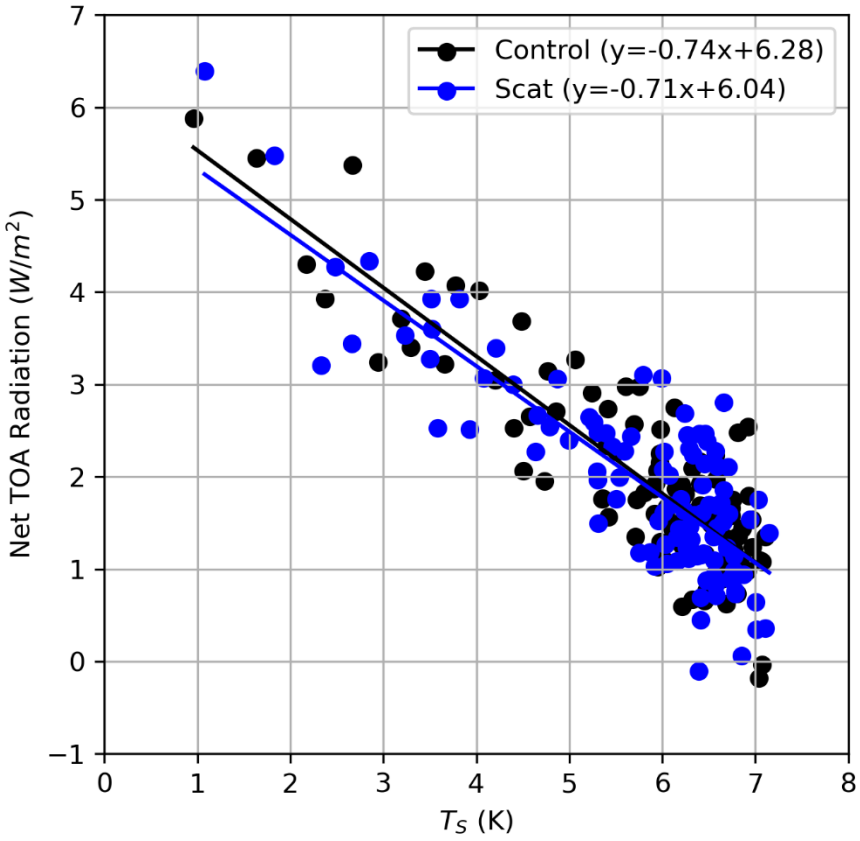

615

616 **Figure 5.** The relationship between the net TOA radiative flux and surface temperature (a.k.a., the

617 Gregory plot) in the Control case (black) and the Scat case (blue). The slope (i.e., climate

618 sensitivity) and the intercept (i.e., ERF) of each regression line are marked in the legend.

619

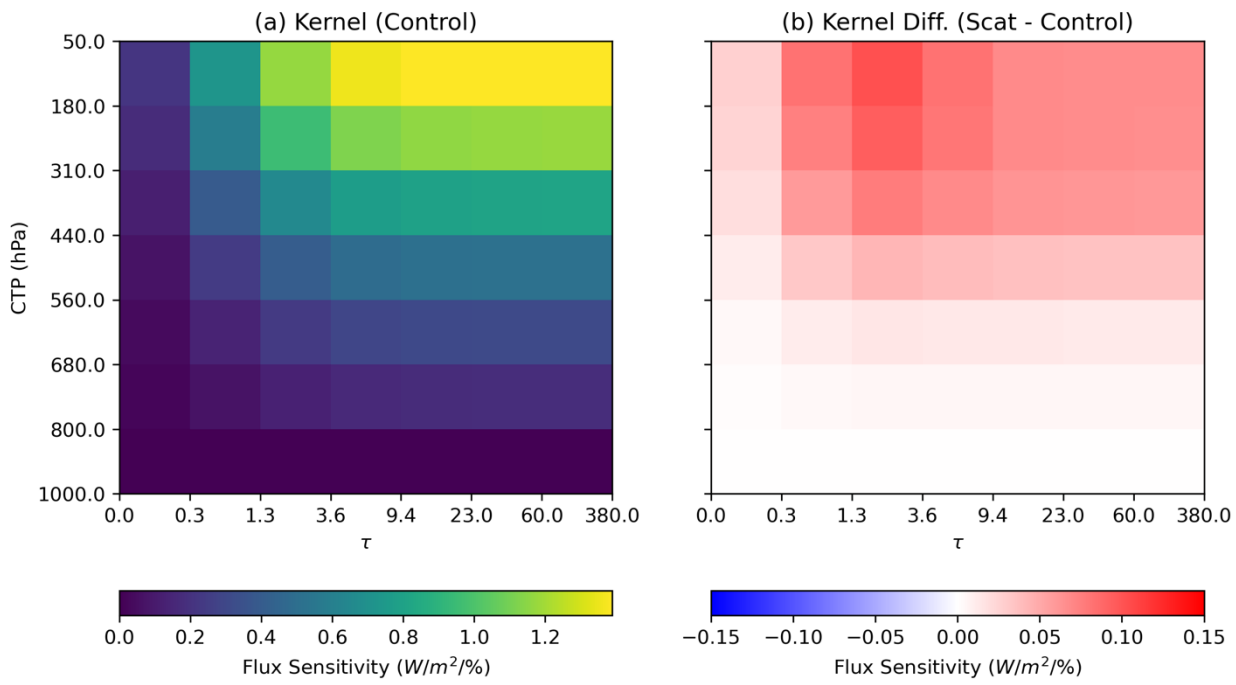

620

621 **Figure 6.** (a) Global and annual mean of the cloud LW radiative kernel we built based on the

622 Control case. (b) The difference of the two kernels based on the Scat case and the Control case

623 (i.e., the correction term). τ is cloud optical thickness at a visible wavelength, and CTP is cloud

624 top pressure. Flux sensitivity is defined as the TOA flux change when we put a cloud with a specific

625 optical thickness at a specific pressure level (net downward is positive).

626

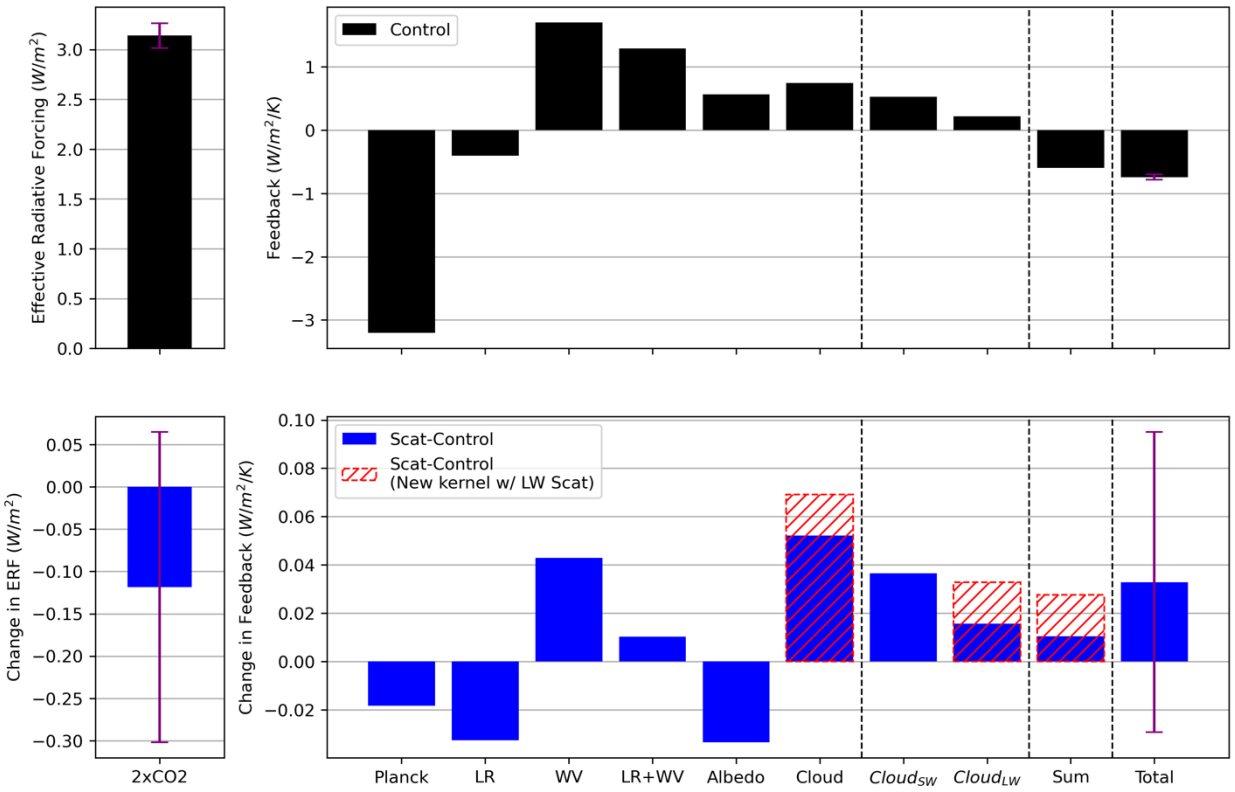

627

628 **Figure 7.** Effective radiative forcing and climate feedbacks estimated from the abrupt 4×CO_2
629 experiment with and without cloud LW scattering. The first row shows the absolute quantities in
630 the Control case, while the second row shows the differences between the Scat case and the Control
631 case. Values of 2xCO_2 ERF and total feedback are estimated from linear regression, while other
632 values are from radiative kernel analysis. The standard errors associated with the linear regression
633 in the Gregory plot (Fig. 5) are attached as purple stems on the corresponding terms. As usual,
634 standard errors of the differences between Scat and Control are the Euclidean norm of the errors
635 in both cases (i.e., $\varepsilon_{diff} = (\varepsilon_{Control}^2 + \varepsilon_{Scat}^2)^{\frac{1}{2}}$). Red slat bars in the second row show the updated
636 values using the corrected cloud radiative kernel (i.e., when cloud LW scattering is considered).

637

638

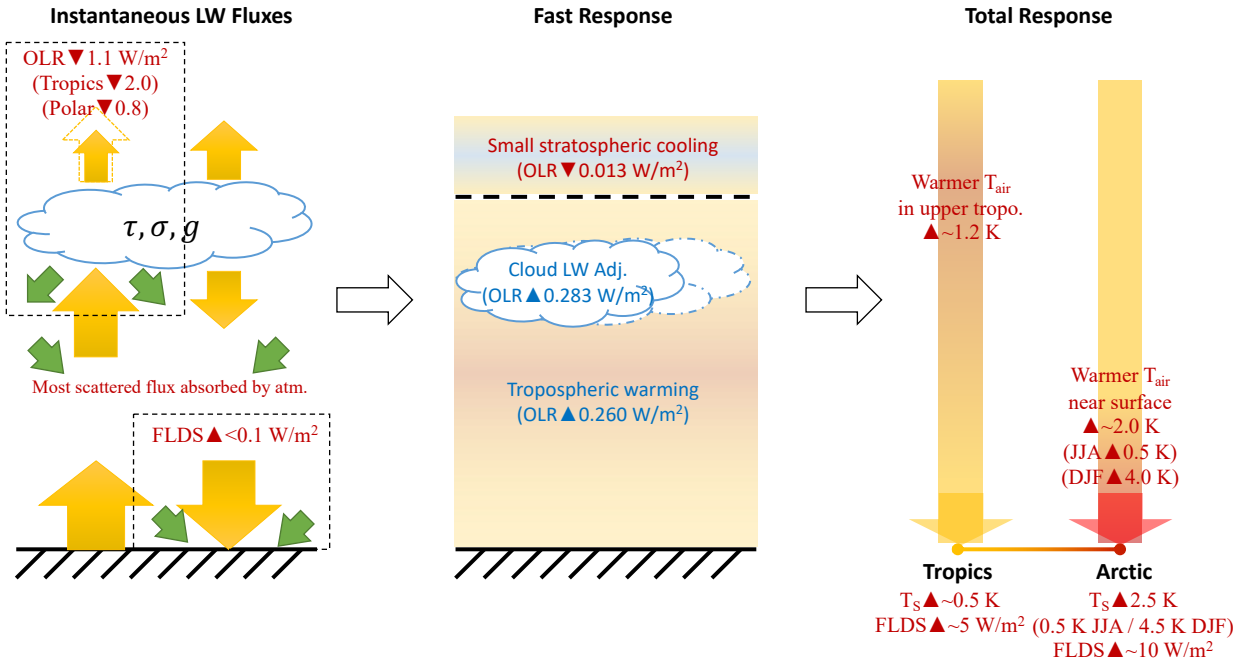

639

640 **Figure 8.** Schematic summary of the instantaneous radiative effect (left), fast response (middle),
641 and total responses (right) due to the inclusion of cloud LW scattering in the E3SMv2. Only
642 prominent features are presented in the diagram. All red texts indicate a warming factor (i.e.,
643 increasing temperature and reducing OLR), while blue texts indicate a cooling factor (i.e.,
644 decreasing temperature and increasing OLR).